Eng. Sci., 2022, **20**, 134–143

Engineered Science

DOI: https://dx.doi.org/10.30919/es8d673

Preparation and Performance of In Situ Carbon-Coated Silicon Monoxide@Carbon@Carbon Microspheres Composite Anode Material for Lithium-Ion Batteries

Lingtong Meng,[2, 3] Chunping Hou,[1, 2,*] Jiao Hou,[3] Haidong Xie,[1] Zeyu Yue,[1] Hui Lu,[1, 2] Shaolin Yang[1, 2] and Bolin Gong[3,*]

Abstract

Silicon monoxide (SiO)@carbon (C)@carbon microspheres (CMSs) composites with core-shell structures were prepared by the hydrothermal method combined with subsequent heat treatment, using glucose as a carbon source. scanning electronic microscopy (SEM) analysis showed that this process resulted in SiO particles that were uniformly coated by the pyrolytic carbon layer and surrounded by CMSs. With increasing quantities of glucose added, the cycle performances of SiO@C@CMSs composites were improved remarkably, with a moderate amount of glucose addition resulting in the greatest performance. Specifically, among the four composite samples, SiO@C@CMSs-2 had the best cycle performance, delivering a high initial capacity of 1024.5 mAh g^{-1} at 50 mA g^{-1} and a specific capacity of 638.6 mAh g^{-1} after 60 cycles at a current density of 200 mA g^{-1}. Even at a current density of 1.5 A g^{-1}, it was still able to deliver a reversible capacity of about 450 mAh g^{-1}. This was attributed to the formation of mesoporous carbon coating and CMSs by the hydrothermal synthesis of glucose. The mesoporous pyrolytic carbon coating of glucose increases the lithium ion diffusion rate and improves the conductivity of the material. At the same time, the volume expansion of the material during lithiation/delithiation is restrained by carbon coating and the CMSs serve as a buffer to alleviate volumetric stress. Therefore, SiO@C@CMSs-2 is a stable material with improved cycle performance.

Keywords: Lithium-ion battery; Anode materials; Composites; Hydrothermal method; Silicon monoxide.
Received: 16 February 2022; Revised: 13 March 2022; Accepted: 16 March 2022.
Article type: Research article.

1. Introduction

Lithium-ion batteries (LIBs) have been widely used in electric vehicles, portable electronic devices, power tools, medical electronics, and other fields. They are valued for their high energy density, high power density, long cycle life, absence of memory effect, low self-discharge rate, wide operating temperature range, safety, and environmental sustainability.[1-4] The anode is the key component of lithium-ion batteries, and improving the performance of anode materials is an effective way to improve the performance of lithium-ion batteries.[5-7] At present, graphite is the commonly used anode material; it has many advantages such as low cost, high conductivity, and good cycle stability. However, graphite anode materials are limited by low theoretical specific capacity (372 mAh g^{-1}), poor charge and discharge performance at high rates, and a tendency toward degradation of cycle performance due to co-embedding of organic solvents.[8-10] By contrast, silicon has a higher theoretical specific capacity (4200 mAh g^{-1}), lower delithiated potential, and abundant reserves, and has therefore recently become a research topic of great interest.[11-13] However, the volume of silicon changes by over 300% during the lithiation/delithiation process, leading to structural damage and rapid reduction of lithiation ability. As a result, the material becomes powdered and peels off from the collector, resulting in loss of effective electrical contact. At the

[1] *College of Materials Science and Engineering, North Minzu University, Yinchuan, Ningxia, 750021, China.*

[2] *Ningxia Silicon Target & Silicon Carbon Anode Material Engineering Technology Research Center, Yinchuan, Ningxia, 750021, China.*

[3] *College of Chemistry and Chemical Engineering, North Minzu University, Yinchuan, Ningxia, 750021, China.*

**Email:* hcp400@163.com (C. Hou); gongbolin@163.com (B. Gong)

same time, the repeated expansions and shrinkages prevent the electrode material from forming a stable solid electrolyte interface (SEI) film. As outer layers of material are lost, the newly-exposed silicon surface forms a new SEI again and again, which will continue to consume lithium ions from the electrolyte and cathode, resulting in reduced coulombic efficiency and accelerated capacity decay.[14-17] Furthermore, silicon is a semiconductor material with low conductivity, which limits the fast transport of lithium ions during high-rate charging and discharging.[18]

The theoretical specific capacity of silicon oxide (SiO_x) is lower than that of silicon, but the generation of inert substances such as lithium oxide (Li_2O) and lithium silicate (Li_4SiO_4) during the lithiation process can alleviate the volume change caused by lithiation/delithiation and increase lithium ion transport. SiO_x also has better cycle stability and is cheaper and easier to prepare than silicon. However, the reaction of SiO_x with lithium ions to form inert substances in the initial cycle is an irreversible process, which will consume some lithium ions and result in a low initial coulombic efficiency; this is another pressing challenge to overcome.

Using dopamine as the carbon source, Hong[19] uniformly coated the surface of nano-silicon particles with an amorphous carbon layer of about 15 nm through *in situ* polymerisation and heat treatment. The carbon layer separated the silicon particles, effectively avoiding particle agglomeration caused by high surface energy. Cao *et al.*[20] prepared a silicon dioxide (SiO_2)/C composite by two-step pyrolysis using D113 resin as the carbon source and ethyl orthosilicate (TEOS) as the silicon source. This ensured the uniform mixing of SiO_2 and carbon and reduced the volume change of SiO_2 during lithiation/delithiation. The SiO_2 and carbon in the composite were both amorphous. Compared with crystalline structures, the volume change of amorphous SiO_2 is smaller, which is beneficial to cycle stability. However, the composite had a low initial coulombic efficiency due to the formation of SEI. The composite had a stable reversible capacity of 1024 mAh g^{-1} at a current density of 100 mA g^{-1} and retained 83% capacity after 100 cycles. Xia *et al.*[21] treated commercial SiO by high-temperature disproportionation and combined it with sucrose to obtain a SiO/C composite. Disproportionation increased the content of Si and decreased the oxygen/silicon value in the composite, thereby reducing the generation of inert Li_2O and Li_4SiO_4 and improving the initial coulombic efficiency. Furthermore, increasing the content of Si can provide a higher specific capacity, and the inert SiO_2 produced by SiO disproportionation can be used as a buffer matrix in lithiation/delithiation, which would significantly improve the cycle stability of the electrodes. The sample showed good electrochemical performance, with an initial charge specific capacity of 933.4 mAh g^{-1} at a current density of 100 mA g^{-1}, and an initial coulombic efficiency of 71%, which increased to close to 100% after 100 charge/discharge cycles.

The hydrothermal method is a simple process involving low reaction temperatures and generating minimal environmental pollution.[22] Materials produced by this method are completely crystalline, do not agglomerate easily and have uniform particle size distributions. In the present study, using glucose as the carbon source, a core-shell SiO@C@carbon microspheres (CMSs) composite anode material was prepared by the hydrothermal method combined with subsequent heat treatment to coat a layer of pyrolytic carbon onto the surface of micron-sized SiO particles and to surround them with hollow carbon microspheres. The SiO particles were coated uniformly by the amorphous carbon in the composite material, which effectively alleviated the volume expansion of the SiO during lithiation/delithiation and improved conductivity. A large number of hollow carbon microspheres were generated during hydrothermal process. These CMSs increase the conductivity of the material, their special hollow spherical structure can reserve space for the volume expansion of SiO and alleviate the structural damage caused by the volume expansion of the SiO anode during lithiation/delithiation to maintain structural stability. In addition, the porous structure of the carbon layer allowed electrolytes to permeate, which can facilitate the transport of lithium ions and thus significantly improve the cycle stability and rate performance of the material.[18,23] Furthermore, a polyoxyethylene copolymer solution (P123) was used as a surfactant in the hydrothermal process. P123 is a non-ionic surfactant composed completely of C, H, and O, and contains few impurities after carbonisation, which allows omission of the washing process after the hydrothermal reaction and simplification of the overall preparation process.

2. Experiment

2.1 Material preparation

Figure 1 illustrated the synthesis of SiO@C@CMSs composite. 0.5 g, 1.0 g, 1.5 g, and 2.0 g of glucose were each dissolved in 50 mL deionized water, then 0.5 g of SiO was dispersed in each of the solutions. Appropriate amounts of surfactant P123 were added to each solution and stirred for 3 h. Solutions were placed in the reactors for the hydrothermal reaction at 200 °C for 12 h, then cooled down to room temperature. Samples were dried at 120 °C. Finally, samples were sintered at 500 °C for 4 h in an argon atmosphere.[18,24] to obtain SiO@C@CMSs composite anode materials with different amounts of carbon coating. The obtained samples, in

order of increasing amounts of carbon, were marked as SiO@C@CMSs-1, SiO@C@CMSs-2, SiO@C@CMSs-3 and SiO@C@CMSs-4. In addition, 1.0 g of glucose was dissolved in 50 mL deionized water, then 0.5 g of SiO was dispersed in the solution, magnetic stirred and dried at the same time, and finally sintered at 700 °C for 4 h in an argon atmosphere to obtain the control sample, marked as SiO@C-0.

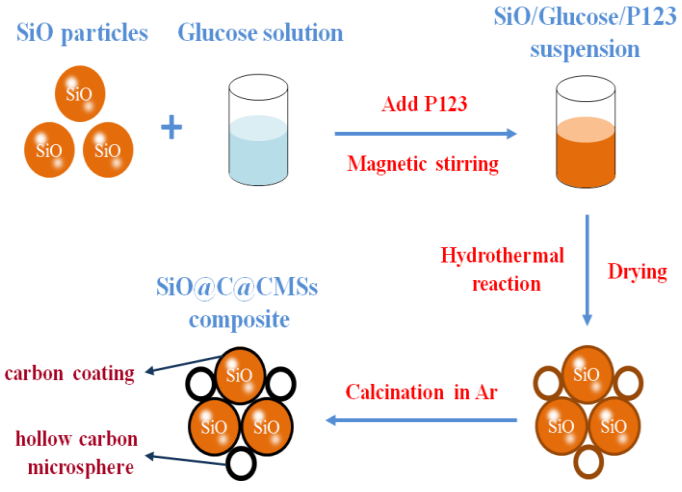

Fig. 1 Synthesis of SiO@C@CMSs composite.

2.2 Characterisation

The surface morphologies of the SiO and SiO@C@CMSs composite were observed by scanning electronic microscopy (SEM; EVO 10, ZEISS) and transmission electron microscopy (TEM; JEM 2100, JEOL). The compositions and structures of the composite were characterised by an X-ray diffractometer (XRD; 6000, Shimadzu) using Cu Kα radiation (λ= 0.154 nm). The specific surface areas, total pore volumes and average pore sizes were determined using a dynamic nitrogen adsorption surface analyser (3H-2000PM1, BEISHIDE).

2.3 Electrochemical measurements

CR2025 coin cells were assembled for the electrochemical measurements. The electrodes were prepared by mixing SiO, SiO@C-0 or SiO@C@CMSs composite with acetylene black and polyacrylic acid (PAA) in a weight ratio of 70:15:15 in deionized water solvent to form a homogeneous slurry. Then, the slurry was uniformly coated onto Cu foil, dried at 80 °C, and punched into a disc of 12 mm diameter. The coin cells were assembled in an argon-filled glove box (LABSTAR 1250/750, MBRAUN). Li foil was used as the counter/reference electrode and Celgard 2400 polypropylene microporous film was used as the separator. The electrolyte was made of 1 M lithium hexafluorophosphate ($LiPF_6$) dissolved in a mixture of ethylene carbonate (EC), diethyl carbonate (DEC) and dimethyl carbonate (DMC) with a volume ratio of 1:1:1. The cells were subjected to galvanostatic charge/discharge tests on a battery testing system (CT-2001A, LAND) with a potential range of 0.01-1.50 V (vs. Li^+/Li). Electrochemical impedance spectroscopy was carried out with an electrochemical workstation (CHI660E, Chenhua) in the frequency range of 10^{-2}-10^5 Hz with a signal amplitude of 5 mV.

3. Results and discussion

3.1 Morphology and structure

Figure 2 shows the X-ray diffractometer (XRD) patterns of SiO, SiO@C-0 and SiO@C@CMSs composites with different amounts of pyrolytic carbon coating. There were no distinct diffraction peaks among the six materials, but they all had several broad diffraction peaks that indicate amorphous characteristics.[18,25] The diffraction peaks of the crystal structure were not obvious. The broad diffraction peaks at around 24° and 51° can be indexed to the characteristic diffraction peaks of amorphous SiO, and the broad diffraction peaks around 22° can be indexed to the (002) plane of the amorphous carbon produced by glucose-coating and *in situ* carbonisation after hydrothermal reaction. With increasing amounts of carbon coating, the broad peaks at around 22° increased gradually in intensity and shifted to smaller degrees. In contrast, the two broad peaks at around 24° and 51° weakened gradually due to the influence of the pyrolytic carbon coating on the diffraction of SiO. The amorphous peak of SiO in the SiO@C-0 pattern is more obvious than that in SiO@C@CMSs because the pyrolytic carbon coating was not uniform and part of SiO was exposed to diffraction, which is consistent with the energy dispersive spectroscopy (EDS) analysis. No other impurity peaks appeared in the patterns of the six samples, indicating that no by-products, such as SiC, were formed.

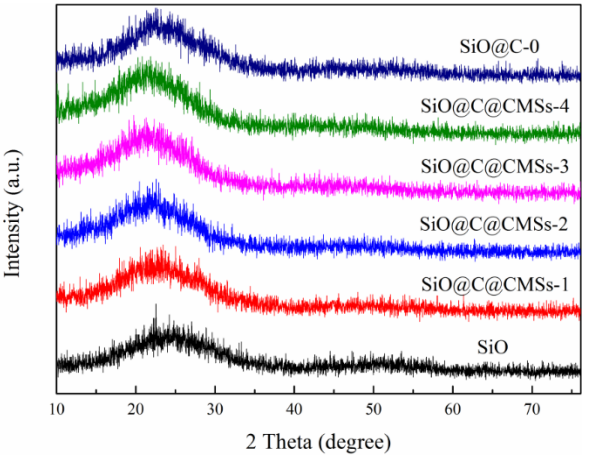

Fig. 2 XRD patterns of SiO, SiO@C-0 and SiO@C@CMSs composites.

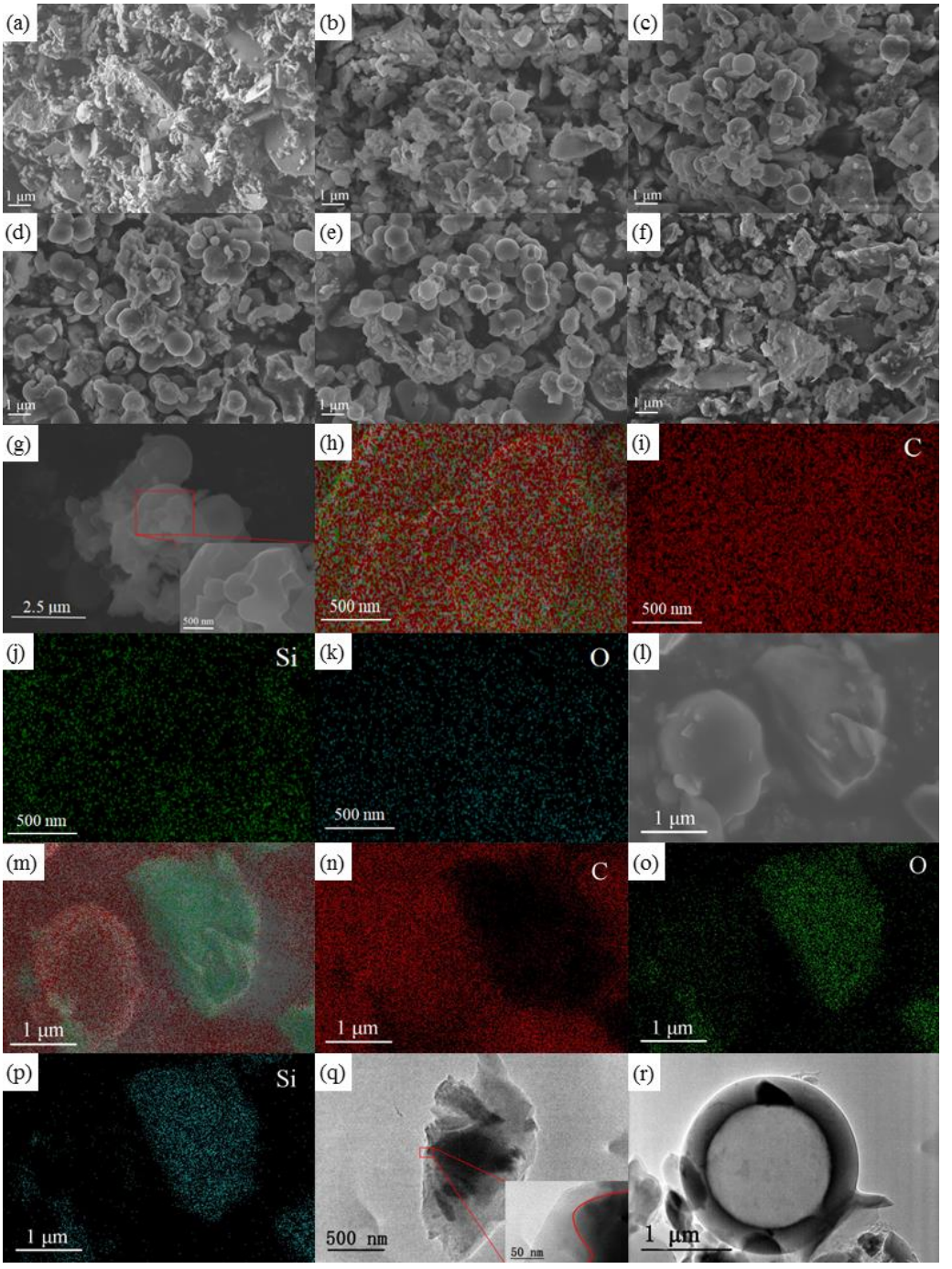

Fig. 3 SEM images of (a) SiO and (b) SiO@C@CMSs-1, (c) SiO@C@CMSs-2, (d) SiO@C@CMSs-3, (e) SiO@C@CMSs-4, (f) SiO@C-0; (g-p) EDS element distribution images of SiO@C@CMSs-2 and SiO@C-0; (q, r) TEM images of SiO@C@CMSs-2.

Figure 3 displays the structures and morphologies of SiO, SiO@C-0 and SiO@C@CMSs composites with different amounts of pyrolytic carbon coating. Fig. 3(a) shows that the SiO particles are irregular in shape, with a size distribution ranging from several hundred nanometres to several microns. As shown in Figs. 3(b)-(e) and (r), there were significantly fewer irregular particles in the SiO@C@CMSs composites prepared by the hydrothermal method, and a large number of hollow carbon microspheres were generated. As increasing amounts of glucose were added, the particles of SiO and CMSs became smaller and more evenly distributed. These CMSs increase the conductivity of the material, and as shown in Fig. 4, their special hollow spherical structure can reserve space for the volume expansion of SiO and alleviate the structural damage caused by the volume expansion of the SiO anode during lithiation/delithiation to maintain structural stability. Fig. 3(f) shows that most of the particles in SiO@C-0 are irregular in shape and do not form hollow carbon microspheres. The EDS element distribution images of SiO@C@CMSs-2 and SiO@C-0 shown in Figs. 3(g)-(p) demonstrate that C, Si,

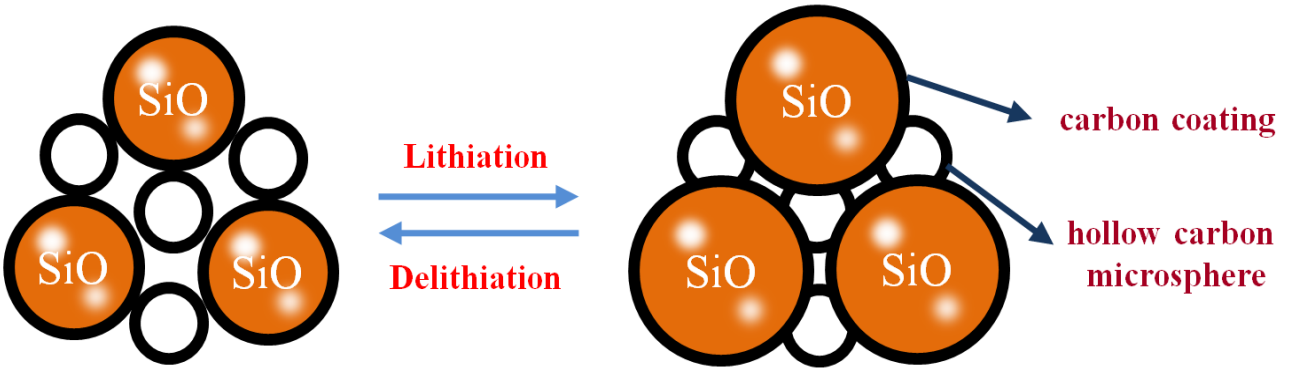

Fig. 4 Schematic diagram of the SiO@C@CMSs reaction process during lithiation/delithiation.

and O elements were distributed uniformly on the particles in SiO@C@CMSs, but not distributed uniformly on the particles in SiO@C-0, indicating that the amorphous carbon layer is uniformly coated on the surfaces of the SiO particles in SiO@C@CMSs, and ununiformly coated on that in SiO@C-0, which is consistent with the results of the XRD patterns. The TEM image of SiO@C@CMSs-2 displayed in Fig. 3(q) further confirms that the SiO@C particles were core-shell structures with SiO as the core surrounded by a 50nm-thick coating of amorphous carbon. The amorphous carbon layer can suppress the volume change of the material during lithiation/delithiation to maintain structural stability, and the porous structure in the carbon layer can improve the diffusion rate of lithium ions and the electron conductivity of the material.[18]

As SiO@C@CMSs-2 showed superior electrochemical performance, including much higher delithiation capacity and excellent cycle performance, SiO@C@CMSs-2, SiO@C-0 and SiO were used to conduct N_2 adsorption-desorption tests. The pore structures of their carbon coatings and the CMSs were also studied. Fig. 5 displays the N_2 adsorption-desorption isotherm of SiO, SiO@C-0 and SiO@C@CMSs-2. The quantity of SiO@C@CMSs-2 and SiO@C-0 adsorbed increased rapidly at low pressures, indicating that they had strong forces with nitrogen, and that the samples contain some microporous structure. The quantity of SiO@C@CMSs-2 adsorbed increased faster at low pressures than that of SiO@C-0, indicating that SiO@C@CMSs-2 contain more microporous than SiO@C-0. Hysteresis loops were present in the adsorption-desorption isotherms of three samples, which indicate that different degrees of capillary condensation occur in each sample and that they had obvious mesoporous structures.[18] The isotherm showed no obvious saturated adsorption platforms, demonstrating that the pore structures in the three samples were irregular. The quantity of material adsorbed was increased by pyrolytic carbon coating, indicating an increase in the total pore volume of the material. This is consistent with the results from pore structure analysis of the three samples.

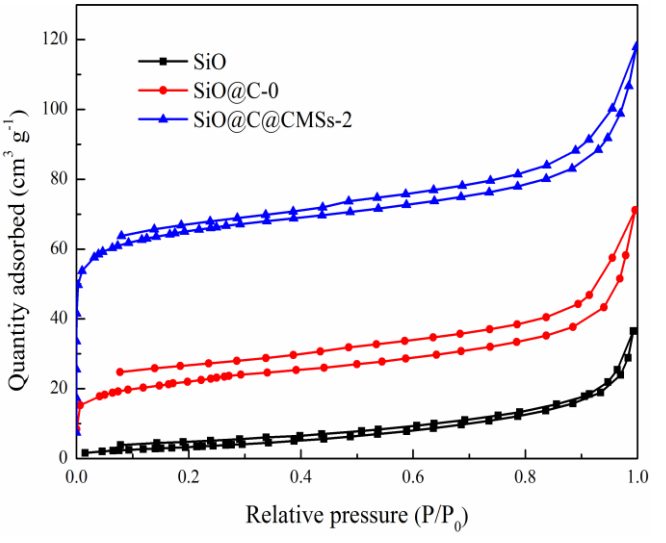

Fig. 5 N_2 adsorption-desorption isotherm for SiO, SiO@C-0 and SiO@C@CMSs-2.

Table 1. Pore structure parameters for SiO, SiO@C-0 and SiO@C@CMSs-2.

Sample	Specific Surface Area (m^2 g^{-1})	Total Pore Volume (cm^3 g^{-1})	Average Pore Size (nm)
SiO	13.4357	0.0565	16.8209
SiO@C-0	74.8931	0.1101	5.8804
SiO@C@CMSs-2	206.995	0.1823	3.5228

Table 1 shows the specific surface areas, total pore volumes, and average pore sizes of the SiO, SiO@C-0 and SiO@C@CMSs-2, as determined by the multipoint BET method. The porous structure of the pyrolytic carbon coating significantly increased the specific surface area and total pore volume of the SiO@C-0 and SiO@C@CMSs-2 composite compared with SiO. The pore size in the pyrolytic carbon layer was small, so the average pore size of the SiO@C-0 and SiO@C@CMSs-2 composite was smaller than that of SiO, which is consistent with the results of the N_2 adsorption-

desorption isotherms. The specific surface area of lot of porous hollow carbon microspheres through hydrothermal synthesis. The porous structure of the composite can enhance the diffusion rate of lithium ions and improve the conductivity of the material. However, the increase in the specific surface area of the material would also increase the contact area with the electrolyte. This would cause more SEI film formation and greater irreversible capacity, resulting in a reduction in the initial coulombic efficiency of the composite.[25]

3.2 Electrochemical measurements

Figure 6(a) shows the cycle performance curves of SiO, SiO@C-0 and SiO@C@CMSs composites with different amounts of pyrolytic carbon coating measured over a potential range of 0.01-1.50 V (vs. Li^+/Li), and the Table 2 shows the initial cycle performances of SiO, SiO@C-0 and SiO@C@CMSs composites. The current densities of the initial 2 cycles and the third and fourth cycles were 50 mA g^{-1} and 100 mA g^{-1} respectively; these were used to activate the electrodes before testing 60 cycles at a current density of 200 mA g^{-1}. Although the initial delithiation capacity of SiO was as high as 1266.9 mAh g^{-1}, it was difficult to maintain a stable internal structure of the material due to the large volume change that occurred during the lithiation/delithiation processes, resulting in structural collapse and the loss of delithiation capacity. At the same time, the formation of many unstable SEI films on the surface of the SiO particles resulted in the loss of effective electrical contact between the material, the collector and the particles within the material. This accelerated the decay in capacity such that the reversible capacity was less than 100 mAh g^{-1} after 30 cycles. The cycle performance of SiO@C-0 was improved compared with that of SiO, but the pyrolytic carbon coating on the particle in SiO@C-0 is not uniform enough to limit the volume change of SiO during the lithiation/delithiation processes, so the cycle performance improvement of SiO@C-0 is limited. The cycle performance of the SiO@C@CMSs-2 composite was significantly improved compared with that of SiO and SiO@C-0, the pyrolytic carbon layer synthesized by hydrothermal synthesis was coated uniformly on SiO particles and inhibited the volume change stress of SiO, which avoided serious damage to the structure of the material, assisted the formation of a stable SEI film, and improved the cycle stability of Si.[26] Simultaneously, micrometre-scale carbon spheres formed during hydrothermal synthesis acted as a buffer to greatly alleviate the volume change stress.

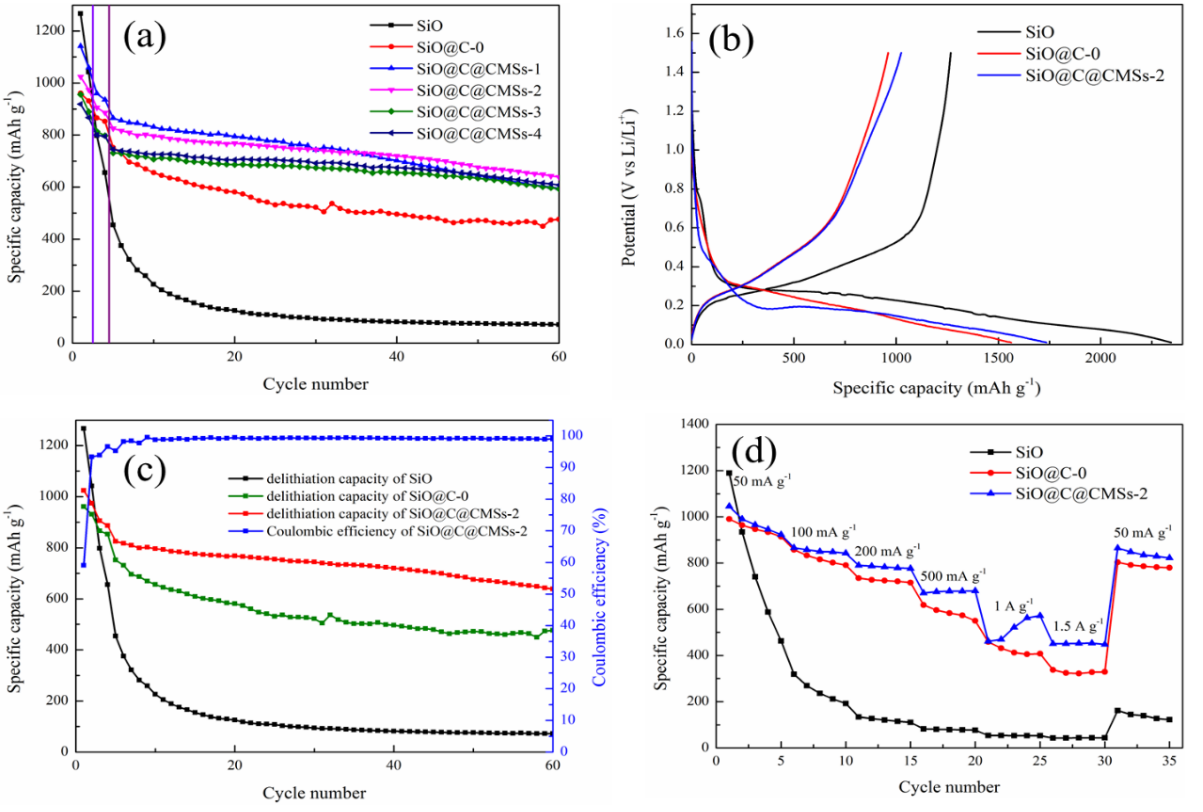

Fig. 6 (a) Cycle performances of SiO, SiO@C-0 and SiO@C@CMSs composites; (b) first charge-discharge curves of SiO, SiO@C-0 and SiO@C@CMSs-2 at a current density of 50 mA g^{-1}; (c) coulombic efficiencies and cycle performances of SiO, SiO@C-0 and SiO@C@CMSs-2; (d) rate performances of SiO, SiO@C-0 and SiO@C@CMSs-2.

Table 2. Initial cycle performances of SiO, SiO@C-0 and SiO@C@CMSs composites.

Sample	Delithiation capacity (mAh g^{-1})	Lithiation capacity (mAh g^{-1})	Initial coloumbic efficiency (%)
SiO	1266.9	2344.5	54.04
SiO@C-0	960.7	1562.2	61.50
SiO@C@CMSs-1	1141.8	1923.7	59.35
SiO@C@CMSs-2	1024.5	1735.1	59.05
SiO@C@CMSs-3	956.3	1663.3	57.49
SiO@C@CMSs-4	918.8	1585.5	57.95

Generally, the cycle performances and rate capabilities of SiO@C@CMSs samples were improved both by carbon coating and carbon microspheres. However, the cycle performances of the SiO@C@CMSs composites with different amounts of pyrolytic carbon coating were quite different. The SiO@C@CMSs-1 sample had the least pyrolytic carbon coating and carbon microspheres, more uncoated SiO particles, and therefore its carbon layer had a poor effect on inhibiting the internal volume expansion of SiO. On the other hand, the excess of pyrolytic carbon coating and CMSs in SiO@C@CMSs-3 and SiO@C@CMSs-4 caused more redundant space, because the capacity of the pyrolytic carbon was much lower than that of SiO, resulting in a lower overall capacity. Among these samples，SiO@C@CMSs-2 had the highest capacity and the best cycle performance, with an initial specific delithiation capacity of up to 1024.5 mAh g^{-1}, a specific delithiation capacity of as high as 638.6 mAh g^{-1} after 60 cycles at a current density of 200 mA g^{-1}, and a capacity retention rate of 77.37% compared with the initial cycle at a current density of 200 mA g^{-1}.

Since SiO@C@CMSs-2 showed good electrochemical performance, the SiO@C@CMSs-2, SiO@C-0 sample and SiO were chosen for further analysis and comparison. Fig. 6(b) shows the charge-discharge curves for SiO, SiO@C-0 and the SiO@C@CMSs-2 composite in the initial cycle, measured in a potential range of 0.01-1.50 V (vs. Li^+/Li) at a current density of 50 mA g^{-1}. The lithiation/delithiation reaction process of SiO_x and amorphous carbon are shown as Formulas (1)-(4).[27] Although the initial lithiation capacity of SiO was as high as 2344.5 mAh g^{-1}, it reacts irreversibly with lithium ions to form inert Li_2O and Li_4SiO_4 [Formulas (1) and (2)], while also reacting with the electrolyte to form SEI film and consuming a large quantity of lithium ions, resulting in a low initial coulombic efficiency of 54.04%. The SiO@C-0 and SiO@C@CMSs-2 sample had a porous structure with a pyrolytic carbon coating layer, which avoids direct contact between the active material and the electrolyte to form stable SEI films. The initial coulombic efficiency of SiO@C@CMSs-2 was increased compared to that of SiO, but slightly lower than that of SiO@C-0, because the specific surface area of SiO@C@CMSs-2 is larger than that of SiO@C-0, this would increase the contact area with electrolyte, resulting in more SEI film formation and greater irreversible capacity, which is consistent with the results from pore structure analysis. Fig. 6(b) shows that during the initial lithiation process of three samples, the rate of increase in potential slowed at about 0.75 V, corresponding to the formation of the SEI film on the material interface. The inclined curve between 0.6 V and 0.25 V corresponds to the formation of Li_2O, Li_4SiO_4 and Si [Formulas (1) and (2)]. The long plateau below 0.25 V corresponds to the intercalation reaction of amorphous carbon and the alloying process of Si [Formulas (3) and (4)].[28] In the initial delithiation process, the plateau above 0.25 V corresponds to the delithiation of amorphous carbon and dealloying of Si, which is the reverse of the reactions shown in Formulas (3) and (4). The potential difference between the charge and discharge curves of SiO@C@CMSs-2 was increased compared to that of SiO, and the initial lithiation of SiO@C@CMSs-2 in the potential range of 0.25-0.15 V showed a potential decrease at first, followed by a slight increase, and then a slow decrease. This is due to the contact between the porous pyrolytic carbon layer and the electrolyte, resulting in more inert SEI film formation and aggravating the polarization of the electrode during the charge-discharge process.

$$SiO_x + 2x\ Li^+ + 2x\ e^- \rightarrow Si + x\ Li_2O \quad (1)$$

$$4\ SiO_x + 4x\ Li^+ + 4x\ e^- \rightarrow (4-x)\ Si + x\ Li_4SiO_4 \quad (2)$$

$$Si + y\ Li^+ + y\ e^- \rightleftharpoons Li_ySi \quad (3)$$

$$C + z\ Li^+ + z\ e^- \rightleftharpoons Li_zC \quad (4)$$

Figure 6(c) shows the coulombic efficiencies and cycle performance curves of SiO, SiO@C-0 and SiO@C@CMSs-2. The coulombic efficiency of the SiO@C@CMSs-2 composite continued to increase after the formation of a stable SEI film on the anode surface by the initial lithiation/delithiation process. Specifically, the coulombic efficiency increased to 96.6% in the fourth cycle and remained above 99% for 9 cycles. Fig. 6(d) shows the rate performance curves of SiO, SiO@C-0 and SiO@C@CMSs-2. The delithiation capacity of SiO, SiO@C-0 and the SiO@C@CMSs-2 composite at the fifth cycle at a current density of 50 mA g^{-1} were 462.8 mAh g^{-1}, 914.3 mAh g^{-1} and 922.7 mAh g^{-1} respectively. As the current density increases, the lithium ion and electron transfer impedance during lithiation/delithiation also increase, which decreases the quantity of lithium ions participating in lithiation/delithiation, thus resulting in a gradual decrease in the specific capacity of the composite. When the current

increased to 1 A/g, the specific capacity of SiO@C@CMSs-2 decreased rapidly because the current increased suddenly. With the activation of charge/discharge for several cycles, the specific capacity of the composite gradually recovers. The reversible capacity of the composite was maintained at about 450 mAh g^{-1} when the current density was increased to 1.5 A g^{-1}, which is nearly 50 % of the reversible capacity at the lower current density of 50 mA g^{-1}. In contrast, the SiO and SiO@C-0 retained a capacity of only about 35 mAh g^{-1} and 325 mAh g^{-1} at a current density of 1.5 A g^{-1} respectively. The delithiation capacities of SiO, SiO@C-0 and SiO@C@CMSs-2 were restored to 161.4 mAh g^{-1}, 803.2 mAh g^{-1} and 864.6 mAh g^{-1} respectively when the current density was decreased to 50 mA g^{-1}, and the recovery rates were close to 35%, 88% and 94% respectively. Taken together, these data indicate that the SiO@C@CMSs-2 composite has good structural stability and rate performance.

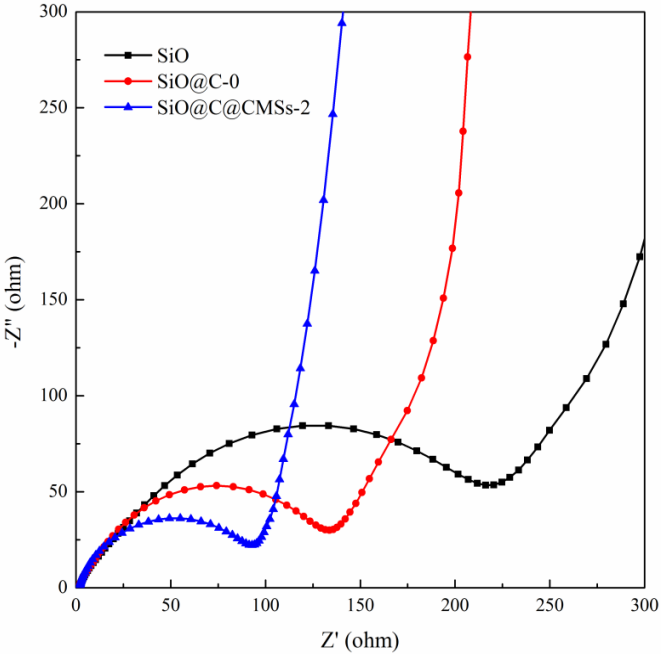

Fig. 7 Nyquist plots of SiO, SiO@C-0 and SiO@C@CMSs-2.

As shown in Fig. 7, Electrochemical Impedance Spectroscopy (EIS) was employed to investigate the effect of the carbon coating layer and carbon microspheres on the electrical resistance of the electrodes by analysing the impedance of the SiO, SiO@C-0 and SiO@C@CMSs-2 composite electrodes. In the Nyquist plot, the compressed semicircle in the high- and middle-frequency regions correspond to the surface film resistance and the charge transfer resistance. The sloped straight line in the low-frequency region is related to the lithium ion diffusion impedance.[29] A smaller diameter of the semicircle indicates smaller surface film resistance and charge transfer resistance; a larger slope of the line indicates lower lithium ion diffusion impedance.[30] The surface film resistance and charge transfer resistance of SiO@C@CMSs-2 were significantly smaller than those of SiO and SiO@C-0, indicating that *in situ* pyrolytic carbon-coating of SiO and hollow carbon microspheres through hydrothermal synthesis enhanced the conductivity of the composite. Meanwhile, the lithium ion diffusion impedance of SiO@C@CMSs-2 and SiO@C-0 were smaller than that of SiO, indicating that the porous structure of pyrolytic carbon coating increased the diffusion channels of lithium ions, thus increasing the diffusion rate and resulting in good rate performance.

4. Conclusion

The *in situ* carbon-coated SiO@C@CMSs composite was prepared by the hydrothermal method using glucose as the carbon source, and the effects of different amounts of glucose coating on the morphology, structure and electrochemical properties of the composites were investigated. The results showed that the prepared SiO@C@CMSs-2 sample had the best electrochemical performance, with a high initial capacity of 1024.5 mAh g^{-1} at 50 mA g^{-1} and a specific capacity of 638.6 mAh g^{-1} after 60 cycles at a current density of 200 mA g^{-1}. Furthermore, even at a current density of 1.5 A g^{-1}, it still delivered a high reversible capacity of about 450 mAh g^{-1}. The internal stress caused by the volume expansion/shrinkage of the composite during the lithiation/delithiation process was suppressed and alleviated by the pyrolytic carbon layer coated on the surface of SiO and the CMSs produced by the hydrothermal method. Meanwhile, the porous structure of the carbon coating shortened the diffusion path of lithium ions, thus improving the diffusion rate of lithium ions and the electron conductivity of the material. This method is simple, economical, environmentally friendly, and has good prospects for application.

Acknowledgement

The authors wish to acknowledge financial support from Ningxia Natural Science Foundation (grant 2020AAC03199), the Key Research Project of Ningxia Hui Autonomous Region (grant 2021BDE92037), Excellent Talents of North Minzu University (grant 2019KYQD17) and the Key Research Project of North Minzu University (grant 2019KJ08).

Conflict of Interest

There is no conflict of interest.

Supporting Information

Not applicable.

References

[1] H. Lu, J. Y. Li, B. N. Liu, G. Chu, Q. Xu, G. Li, F. Luo, J. Y. Zheng, Y. X. Yin, Y. G. Guo, H. Li, Research and technology progress of nano-Si/C anode materials for lithium ion batteries, *Energy Storage Science and Technology*, 2017, **6**, 864-870.

[2] T. Zhang, J. Gao, H. P. Zhang, L. C. Yang, Y. P. Wu, H. Q. Wu, Preparation and electrochemical properties of core-shell Si/SiO nanocomposite as anode material for lithium ion batteries, *Electrochemistry Communications*, 2007, **9**, 886-890, doi: 10.1016/j.elecom.2006.11.026.

[3] Q. Xiao, M. Gu, H. Yang, B. Li, C. Zhang, Y. Liu, F. Liu, F. Dai, L. Yang, Z. Liu, X. Xiao, G. Liu, P. Zhao, S. Zhang, C. Wang, Y. Lu, M. Cai, Inward lithium-ion breathing of hierarchically porous silicon anodes, *Nature Communications*, 2015, **6**, 8844, doi: 10.1038/ncomms9844.

[4] L.-F. Cui, Y. Yang, C.-M. Hsu, Y. Cui, Carbon−Silicon Core−Shell nanowires as high-capacity electrode for lithium-ion batteries, *Nano Letters*, 2009, **9**, 3370-3374, doi: 10.1021/nl901670t.

[5] H. Chang, Y. R. Wu, X. Han, T. F. Yi, Recent progress of advanced anode materials of lithium-ion batteries, *Journal of Energy Chemistry*, 2021, **6**, 451-468, doi: 10.1016/j.jechem.2020.08.056.

[6] W. Tu, Z. Bai, Z. Deng, H. Zhang, H. Tang, In-situ synthesized Si@C materials for the lithium-ion battery: a mini review, *Nanomaterials*, 2019, **9**, 432, doi: 10.3390/nano9030432.

[7] J. Han, X. Tang, S. Ge, Y. Shi, C. Zhang, F. Li, S. Bai, Si/C particles on graphene sheet as stable anode for lithium-ion batteries, *Journal of Materials Science & Technology*, 2021, **80**, 259-265, doi: 10.1016/j.jmst.2020.11.054.

[8] M. Yamada, A. Ueda, K. Matsumoto, T. Ohzuku, Silicon-based negative electrode for high-capacity lithium-ion batteries: "SiO"-carbon composite, *Journal of the Electrochemical Society*, 2011, **158**, A417, doi: 10.1149/1.3551539.

[9] T. Yang, H. Ying, S. Zhang, J. Wang, Z. Zhang, W. Q. Han, Electrochemical performance enhancement of micro-sized porous Si by integrating with Nano-Sn and carbonaceous materials, *Materials*, 2021, **14**, 920, doi: 10.3390/ma14040920.

[10] N. Wang, Y.-Y. Liu, Z.-X. Shi, Z.-L. Yu, H.-Y. Duan, S. Fang, J.-Y. Yang, X.-M. Wang, Electrolytic silicon/graphite composite from SiO_2/graphite porous electrode in molten salts as a negative electrode material for lithium-ion batteries, *Rare Metals*, 2022, **41**, 438-447, doi: 10.1007/s12598-020-01702-z.

[11] H. Wu, G. Yu, L. Pan, N. Liu, M. T. McDowell, Z. Bao, Y. Cui, Stable Li-ion battery anodes by in situ polymerization of conducting hydrogel to conformally coat silicon nanoparticles, *Nature Communications*, 2013, **4**, 1943, doi: 10.1038/ncomms2941.

[12] S. Uchida, M. Mihashi, M. Yamagata, M. Ishikawa, Electrochemical properties of non-nano-silicon negative electrodes prepared with a polyimide binder, *Journal of Power Sources*, 2015, **273**, 118-122, doi: 10.1016/j.jpowsour.2014.09.096.

[13] P. Wu, B. Shi, H. Tu, C. Guo, A. Liu, G. Yan, Z. Yu, Pomegranate-type Si/C anode with SiC taped, well-dispersed tiny Si particles for lithium-ion batteries, *Journal of Advanced Ceramics*, 2021, **10**, 1129-1139, doi: 10.1007/s40145-021-0498-6.

[14] L. Shi, C. Pang, S. Chen, M. Wang, K. Wang, Z. Tan, P. Gao, J. Ren, Y. Huang, H. Peng, Z. Liu, Vertical graphene growth on SiO microparticles for stable lithium ion battery anodes, *Nano Letters*, 2017, **17**, 3681-3687, doi: 10.1021/acs.nanolett.7b00906.

[15] Q. Xu, J.-Y. Li, J.-K. Sun, Y.-X. Yin, L.-J. Wan, Y.-G. Guo, Watermelon-inspired Si/C microspheres with hierarchical buffer structures for densely compacted lithium-ion battery anodes, *Advanced Energy Materials*, 2017, **7**, 1601481, doi: 10.1002/aenm.201601481.

[16] C. Back, T. Kim, N. Choi, Activated natural porous silicate for a highly promising SiO_x nanostructure finely impregnated with carbon nanofibers as a high-performance anode material for lithium-ion batteries, *Journal of Materials Chemistry A*, 2014, **2**, 13648-13654, doi: 10.1039/C4TA02706J.

[17] M. Zhang, T. Zhang, Y. Ma, Y. Chen, Latest development of nanostructured Si/C materials for lithium anode studies and applications, *Energy Storage Materials*, 2016, **4**, 1-14, doi: 10.1016/j.ensm.2016.02.001

[18] C. Geng, J. Yu, F. Shi, Synthesis and electrochemical performance of TiO_2/rGO composites with different layers of graphene oxide as anode materials for lithium-ion battery, *IOP Conference Series: Materials Science and Engineering*, 2019, **585**, 012090, doi: 10.1088/1757-899X/585/1/012090.

[19] Z. Luo, D. Fan, X. Liu, H. Mao, C. Yao, Z. Deng, High performance silicon carbon composite anode materials for lithium ion batteries, *Journal of Power Sources*, 2009, **189**, 16-21, doi: 10.1016/j.jpowsour.2008.12.068.

[20] L. Cao, J. Huang, Z. Lin, X. Yu, X. Wu, B. Zhang, Y. Zhan, F. Xie, W. Zhang, J. Chen, H. Meng, Amorphous SiO_2/C composite as anode material for lithium-ion batteries, *Journal of Materials Research*, 2018, **33**, 1219-1225, doi: 10.1557/jmr.2017.298.

[21] W. M. Xia, R. H. Tang, H. Wang, Y. Wang, F. M. Xiao, M. Zhu, T. Sun, High-performance SiO/C anode material in Li-ion battery by pre-disproportionation treatment, *Materials Review*, 2017, **31**, 11-15, doi: 10.1557/jmr.2017.298.

[22] Z. Liao, M. Ma, Z. Tong, Y. Bi, K. L. Chung, M. Qiao, Y. Ma, A. Ma, G. Wu, X. Zhong, R. Sun, Fabrication of one-dimensional $CoFe_2$/C@MoS_2 composites as efficient electromagnetic wave absorption materials, *Dalton Transactions*, 2021, **50**, 11640-11649, doi: 10.1039/d1dt01915e.

[23] Y. Liu, Z. Tong, K. Che, M. Ma, W. Huang, K. L. Chung, Y. Ma, G. Wu, Z. Na, F. Fan, Facile fabrication of porous hexagonal flaky Co@C core-shell composites with excellent microwave-absorbing properties, *Journal of Alloys and Compounds*, 2021, **874**, 159815, doi: 10.1016/j.jallcom.2021.159815.

[24] Z. Ku, Dissertation, Preparation and electrochemical performance of SiO anode materials for lithium-ion batteries. Dissertation, Harbin Engineering University, 2019.

[25] H. Tonnoir, D. Huo, R. L. Canevesi, V. Fierro, A. Celzard, R. Janot, Tannin-based hard carbons as high-performance anode materials for sodium-ion batteries, *Materials Today Chemistry*,

2022, **23**, 100614, doi: 10.1016/j.mtchem.2021.100614.
[26] Y. Tao, L. Xiao, T. X. Dong, S. Yan, L. Z. Jun, G. Q. Gui, Preparation and Electrochemical Performance of Si@C/SiO_x as Anode Material for Lithium-ion Batteries, *Journal of Inorganic Materials*, 2017, **32**, 699-704, doi: 10.15541/jim20160516.
[27] H. Liu, E. Huangzhang, C. Sun, Y. Fan, Z. Ma, X. Zhao, J. Nan, SiO_x/C Composite Anode of Lithium-Ion Batteries with Enhanced Performances Using Multicomponent Binders, *ACS omega*, 2021, **6**, 26805-26813, doi: 10.1021/acsomega.1c04544.
[28] M. Li, Y. Zeng, Y. Ren, C. Zeng, J. Gu, X. Feng, H. He, Fabrication and lithium storage performance of sugar apple-shaped SiO_x@C nanocomposite spheres, *Journal of Power Sources*, 2015, **288**, 53-61, doi: 10.1016/j.jpowsour.2015.04.127.
[29] W. Zheng, P. Zhang, J. Chen, W. B. Tian, Y. M. Zhang, Z. M. Sun, in situ synthesis of CNTs@Ti_3C_2 hybrid structures by microwave irradiation for high-performance anodes in lithium ion batteries, *Journal of Materials Chemistry A*, 2018, **6**, 3543-3551, doi: 10.1039/c7ta10394h.
[30] J. Hou, C.-P. Hou, X.-W. Wang, L.-T. Meng, D. Yang, B.-L. Gong, Cyclic utilisation of waste tires as nanostructured anode materials for Li-ion batteries, *Materials Technology*, 2020, **35**, 612-617, doi: 10.1080/10667857.2020.1723836.

Author Information

Lingtong Meng *obtained his B.S. degree (2017) from College of Chemistry and Materials Science, LiaoNing Petrochemical University. He is currently working toward his Master's degree at North Minzu University. His current research involves the electrode material for lithium-ion batteries (LIB).*

Chunping Hou *obtained his Master of Engineering degree (2006) from Yanshan University and Ph.D. degree (2018) in Materials Science from Northwestern Polytechnical University, respectively. He achieved senior engineer in 2015 and was appointed as CTO in Bolt Technologies Co. Ltd. Since 2018, he has worked in North Minzu University as an associate professor. His main research interests focus on electrochemical energy storage engineering, nanocomposite electrode materials for LIB and carbon-based functional materials.*